ADVANCED MATERIALS

Supporting Information

for *Adv. Mater.*, DOI: 10.1002/adma.201907444

Engineering Oxygen Vacancies in a Polysulfide-Blocking Layer with Enhanced Catalytic Ability

Zhaohuai Li, Cheng Zhou, Junhui Hua, Xufeng Hong, Congli Sun, Hai-Wen Li, Xu Xu, and Liqiang Mai**

Supporting Information

Engineering Oxygen Vacancies in a Polysulfide-Blocking Layer with Enhanced Catalytic Ability

Zhaohuai Li, Cheng Zhou, Junhui Hua, Xufeng Hong, Congli Sun, Hai-Wen Li, Xu Xu, Liqiang Mai**

Experimental section

Preparation of O-TiO_2 and OVs-TiO_2 nanosheets. O-TiO_2 nanosheets were synthesized according to a previous report.[S1] Typical, 3 mL of hydrofluoric acid solution (40 wt%) was slowly added to 25 mL of Tetra-n-butyl titanate, stirring for 2 hours until the solution changed into gel. Then, the gel was transferred to 50 mL teflon reactor and placed at 180 ºC for 36 hours. After the reaction was finished, the sample washed by centrifugation with deionized water and anhydrous ethanol for 3 times, respectively. The obtained samples were retreated with 250 mL of 0.1 M sodium hydroxide solution for 12 hours, followed by centrifugation and deionized water washing, the final sample O-TiO_2 nanosheets were obtained after dry for 1 day at 60 ºC. The OVs-TiO_2 nanosheets were obtained by calcining the O-TiO_2 nanosheets at 200 ºC for 2 hours in hydrogen atmosphere.

Preparation of OVs-TiO_2@PP and O-TiO_2@PP functional separators. The as-obtained OVs-TiO_2 nanosheets were dispersed in absolute ethanol with ultrasonic treatment for more than 2 hours. Then, the homogeneous solution was kept standing for another 2 hours and the supernatant was taken for vacuum filtration to obtain the

uniform OVs-TiO_2 nanosheet coated PP (OVs-TiO_2@PP) separator. Finally, OVs-TiO_2@PP separator was obtained by freeze-drying for 1 day. The O-TiO_2@PP separator synthesized as the same method as OVs-TiO_2@PP separator with O-TiO_2 nanosheets.

Preparation of rGO/S cathode. 0.1 mL sodium thiosulfate solution (1 M) was added to a mixture solution of 1.16 mL of deionized water and 0.26 mL of graphene dispersion solution (3.8 mg mL^{-1}). After stirring, 0.1 mL of hydrochloric acid was slowly added to the above solution and stirred for 2 hours. Then, 0.2 mL of sodium ascorbate solution (1 M) was added, and the mixture was placed at 95 ºC oven for 2 hours. After washing with deionized water for several times, the freestanding rGO/S cathode was obtained by freeze-drying. The high sulfur loading was prepared through increased the sodium thiosulfate solution. The free-standing rGO/S cathode diameter (6 mm) is prepared by the self-assembly, and the normal loading and high loading sulfur contents were 66.7 wt.% and 80 wt.%, respectively.

Shuttle test. The 0.05 M Li_2S_6 solution was prepared by reacting sulfur and Li_2S at a molar ratio of 5:1, which added to precise configured liquid mixture of 1, 2-dimethoxyethane (DME) and 1, 3-dioxolane (DOL) (1:1 in volume) and homogenized by vigorous stirring at 70 ºC for 48 hours. Then, The same volume of 0.05 M Li_2S_6 solution and blank solution were added to the two sides of the proton exchanger container, sealed and tested.

Materials Characterizations. Scanning electron microscopy (SEM) images were obtained by using a JEOL JSM-7100F at a voltage of 15 keV. Transmission electron microscopy (TEM) and high-resolution TEM (HRTEM) images were recorded with a

Titan G2 60-300 with EDS image corrector. X-ray diffraction (XRD) characterization was performed using a D8 Advance X-ray diffractometer with a non-monochromated Cu Ka X-ray source (λ= 1.054056 Å). X-ray photoelectron spectroscopy (XPS) measurements were collected using a VG MultiLab 2000 instrument. X-band electron paramagnetic resonance (EPR) measurement was performed at room temperature using a Bruker spectrometer. Scanning transmission electron microscopy (STEM) and electron energy loss microscopy (EELS) experiments were performed on a FEI Titan microscope with a CEOS probe aberration-corrector operated at 200 keV. The probe semi-angle was 24.5 mrad and the probe current was ~25 pA. The estimated probe size was less than 1 Å. EEL spectrum image were recorded with GIF 865 spectrometer, with energy dispersion of 0.2 eV/pixel, which allowed the simultaneous visualization of the Ti-L and O-K EELS edges.

Theoretical computations. Density functional theory (DFT) as a branch of the first principle theory was applied to estimate the adsorption energies of Li_2S_x ($3 \leq x \leq 8$) on anatase TiO_2 (101) surface and the Li ion transport energy barrier inside TiO_2 bulk. DFT calculations were achieved by Vienna Ab-initio Simulation Package (VASP).[S2] All of the atomic structures involved are fully relaxed with the energy convergence of 5×10^{-5} eV/atom and the internal perpendicular forces were reduced to less than 0.02 eV/Å. The planewave cutoff energy was set to be 550 eV. The projector augmented wave (PAW)[S3] potentials of involved elements and the GGA-PBE exchange-correlation functional were adopted.[S4] The Brillouin zone of the were sampled by a 2 × 2 × 1 uniform k point mesh. Grimme's semiempirical DFT-D3 scheme[S5] of dispersion correction was used

to simulate the van der Waals (vdW) interactions in the layered system for adsorption energy calculations. The Li transport barriers along the path between two most stable sites on TiO_2 (101) surface were simulated by the climbing-image nudged elastic band (CINEB)[S6] method implemented in VASP. The adsorption energy (Ea) is calculated by the equation: $Ea = E(TiO_2 + Li_2S_x) – E(TiO_2)– E(Li_2S_x)$

Electrochemical Measurements. Stainless steel coin cells (2,025-type) were assembled in a glovebox filled with pure argon gas. A Celgard 2400 polypropylene (PP) was used as the normal separator, the OVs-TiO_2@PP and O-TiO_2@PP as functional separator. The electrolyte was 1.0 M lithium bistrifluoromethanesulfonylimide (99.95%, Sigma-Aldrich) dissolved in DOL (99.95%, Sigma-Aldrich) and DME (99.95%, Sigma-Aldrich) (1:1 ratio by volume) with 0.1 M lithium nitrate ($LiNO_3$, 99.9%, Alfa Aesar) as the additive. For the cycling test of both normal and high sulfur loading cells, 15 μL electrolyte is added to both sides of lithium anode and rGO/S cathode, and the total amount of electrolyte in each cell is 30 μL. The cyclic voltammetry (CV), the electrochemical impedance spectra (EIS) and open circuit voltage (OCV) profiles were tested by electrochemical workstation (Autolab PGSTAT302N), and all the assembled cells stand for 6 hours before test. The Galvanostatic charge/discharge and cycling measurements were performed with a multichannel battery testing system (LAND CT2001A) in the potential range from 1.6-2.8 V at different current densities. The cycling tests were performed at low current density for initial few cycles. All the

specific capacities were calculated based on the mass of sulfur.

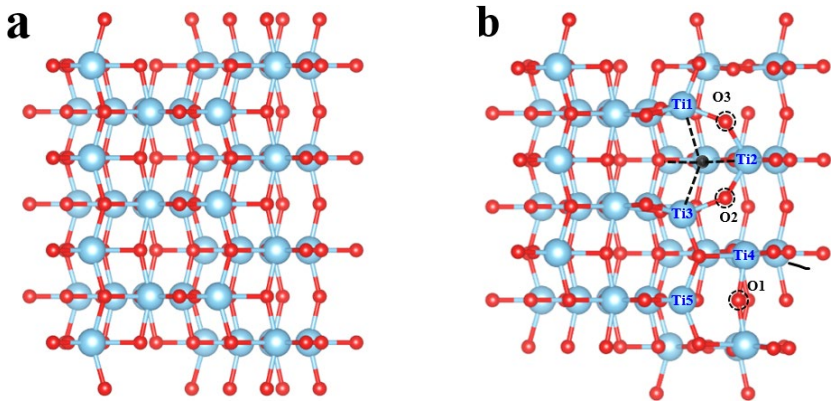

Figure S1. Optimized configurations of (a) O-TiO_2 and (b) OVs-TiO_2.

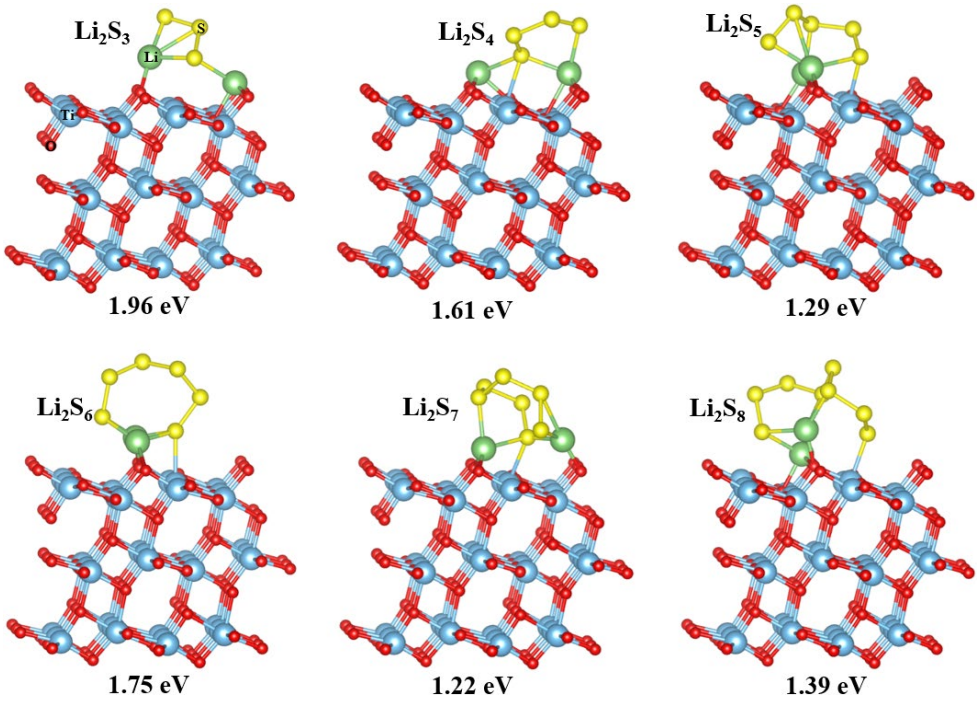

Figure S2. Optimized configurations of polysulfides (Li_2S_x, $3 \leq x \leq 8$) being adsorbed on O-TiO_2 (101) plane.

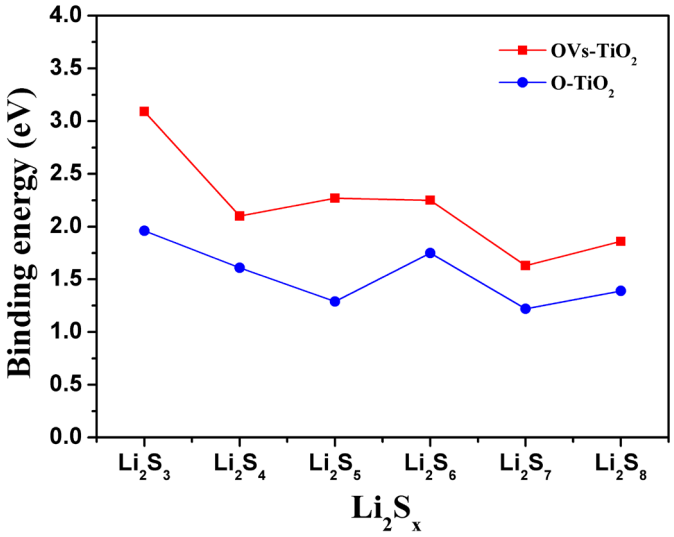

Figure S3. Adsorption energies curves of polysulfides (Li_2S_x, $3 \leq x \leq 8$) on TiO_2 (101) surface with/without O vacancy.

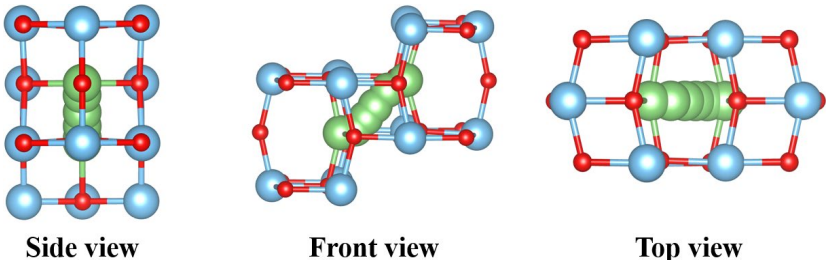

Figure S4. Schematic of Li transport path in O-TiO_2.

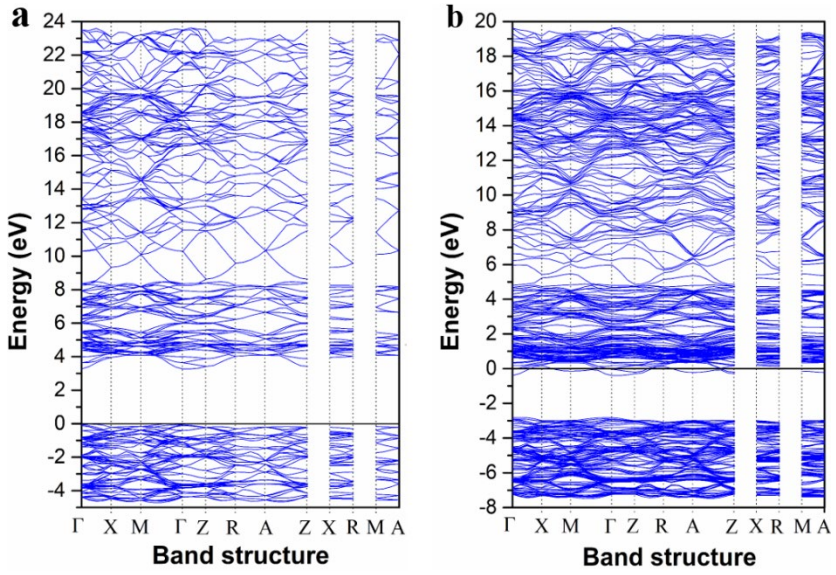

Figure S5. First-principle calculations. DOS of (a) O-TiO_2 and (b) OVs-TiO_2.

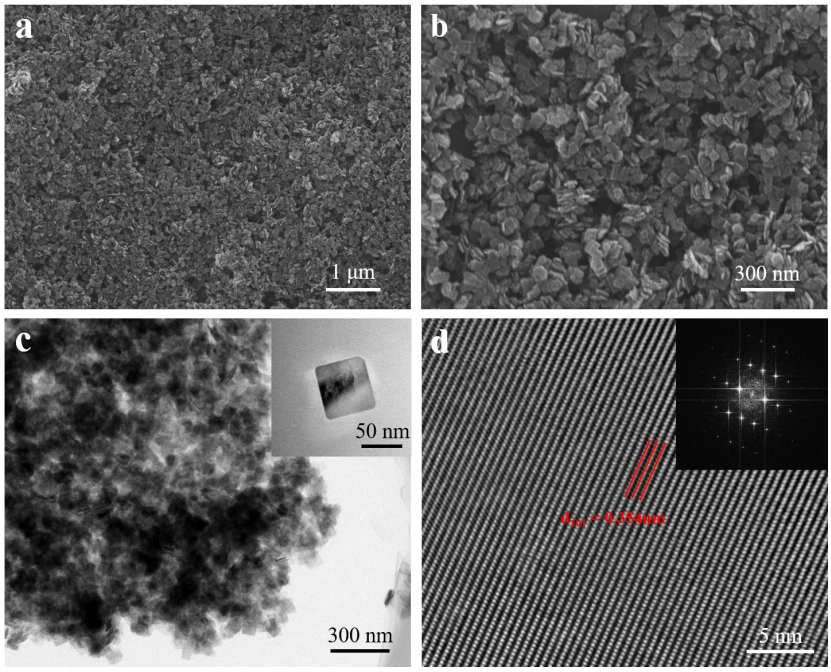

Figure S6. (a, b) SEM, (c) TEM and (d) HRTEM image of the OVs-TiO_2 nanosheets (inset is FFT conversion of d).

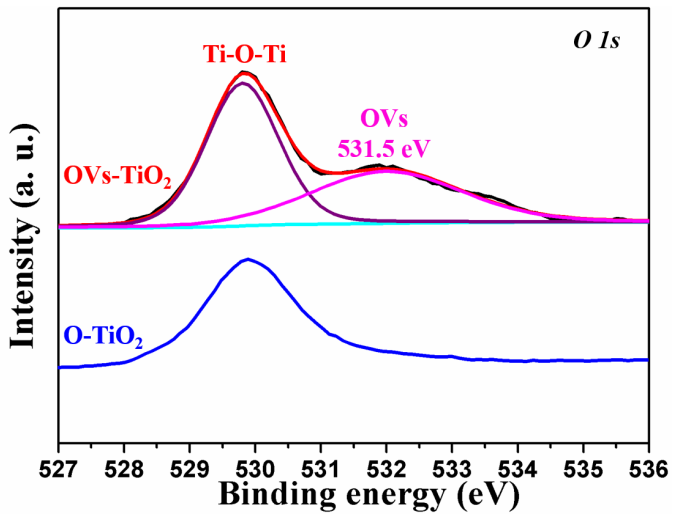

Figure S7. High-resolution XPS spectrum of O 1s of OVs-TiO_2 and O-TiO_2.

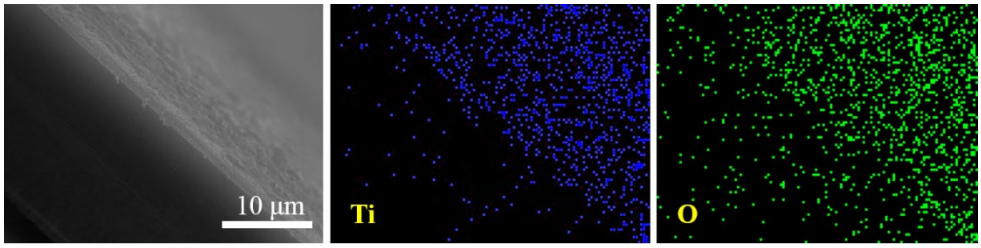

Figure S8. SEM elemental mappings of the OVs-TiO_2@PP separator.

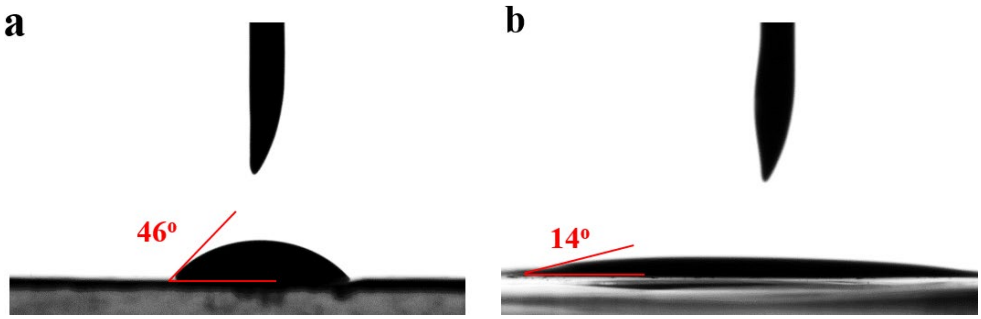

Figure S9. Photographs of electrolyte on (a) a PP separator and (b) an OVs-TiO_2@PP separator.

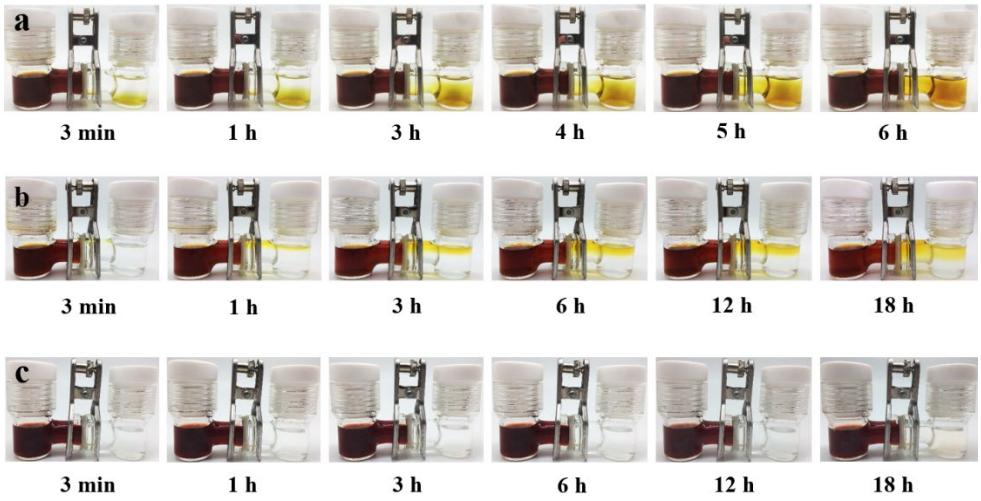

Figure S10. Photographs of proton exchanger with LiPS (Li_2S_6) in DOL/DME solution and pure DOL/DME solvent in the left and right chambers, respectively. (a) PP separator. (b) O-TiO_2@PP separator. (c) OVs-TiO_2@PP separator.

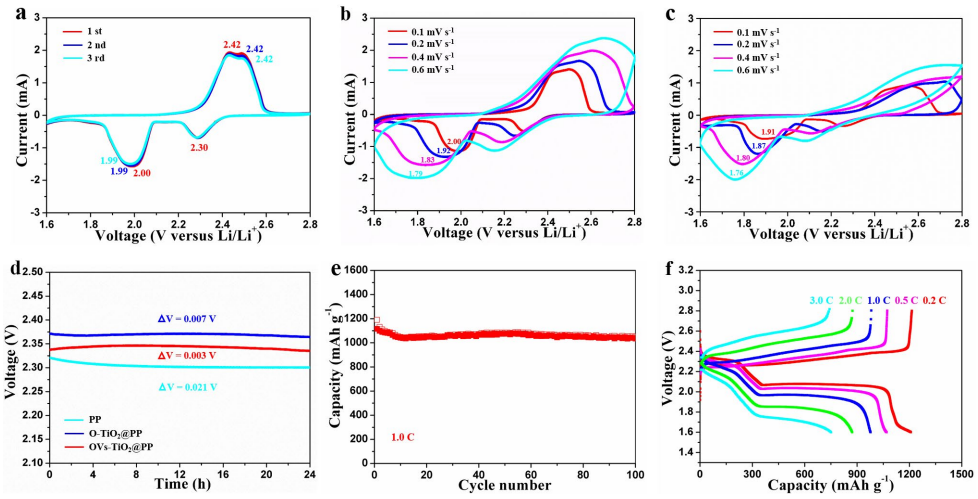

Figure S11. Electrochemical characterizations. (a) Initial three CV curves of the OVs-TiO_2@PP at 0.2 mV S^{-1}. Multi-scan CV curves of (b) O-TiO_2@PP and (c) PP separators, respectively. (d) The OCV curves of OVs-TiO_2@PP, OTiO_2@PP and PP separators, respectively. (e) Cycling performance of the OVs-TiO_2@PP separator at a current density of 1 C. (f) Charge and discharge curves of OVs-TiO_2@PP separator under different current densities.

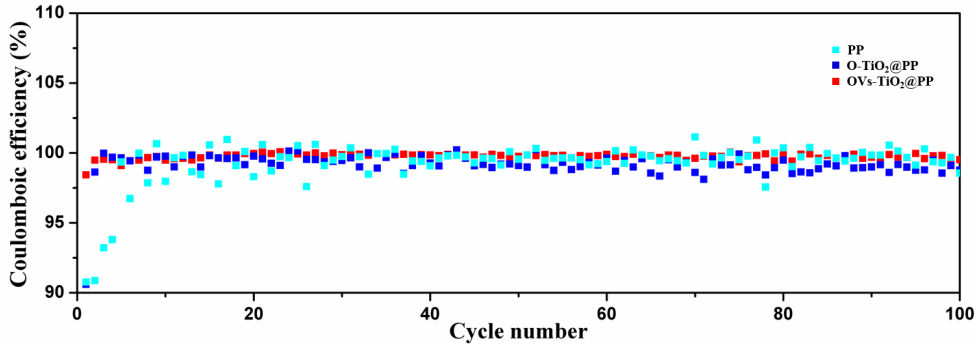

Figure S12. Coulombic efficiencies of the OVs-TiO_2@PP, O-TiO_2@PP, and PP separators at the current density of 0.5 C.

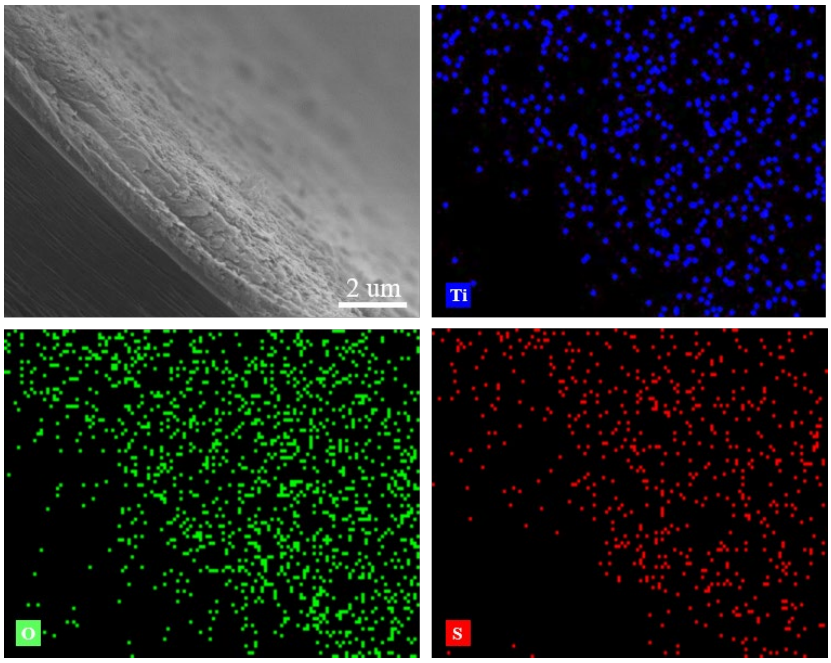

Figure S13. SEM image and corresponding elemental mappings of OVs-TiO_2@PP after cycled.

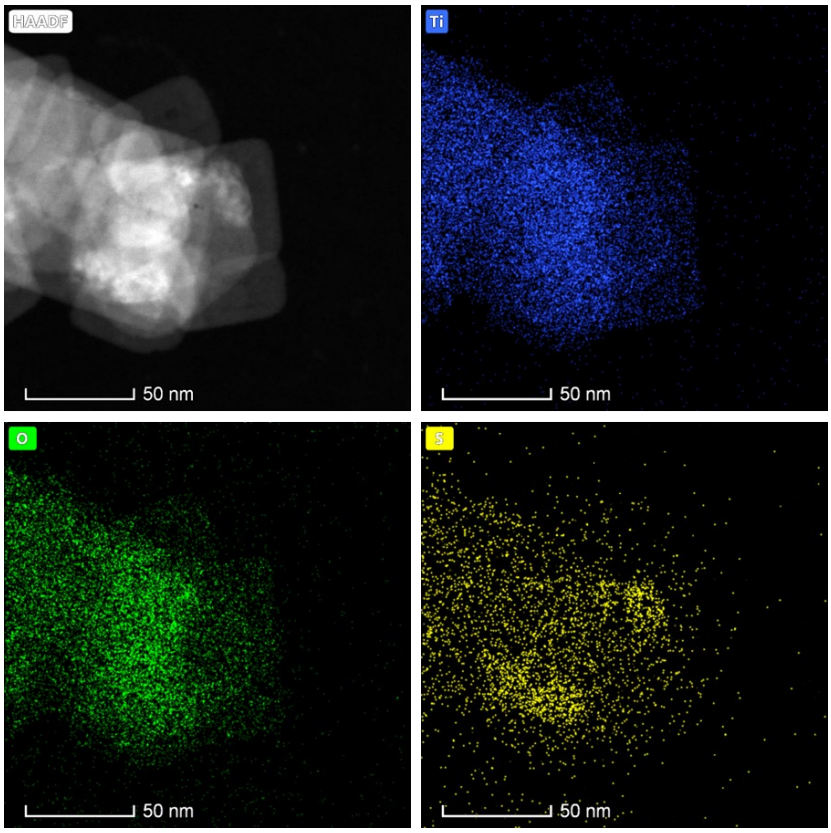

Figure S14. STEM mappings of OVs-TiO_2 form OVs-TiO_2@PP separator after cycled.

Table S1. Battery parameters comparison of metal-based coating modified separator in Li-S battery.

Coating Materials	Thickness / Loading (μm / mg cm^{-2})	Sulfur Loading (mg cm^{-2})	Sulfur content (wt%)	Rate (1C = 1675 mA g^{-1})	Capacity (mAh g^{-1})	Operation voltage window (V)	Areal capacity (mAh cm^{-2})	Ref.
OVs-TiO_2	**0.5 / 0.12**	**3.6**	**66.7**	**0.5 C**	**1148 (100 cycles)**	**1.6-2.8**		**This Work**
				2.0 C	**631 (500 cycles)**			
		7.1	**80**	**2.4 mA cm^{-2}**	**821 (100 cycles)**		**5.83**	
MWCNTs@TiO_2	0.5 / —	0.8-1.0	—	0.5 C	610 (600 cycles)	1.8-2.6	—	S7
Carbon/TiO_2	4.0 / 0.2	2.0	63	0.5 C	750 (200 cycles)	1.7-2.8	—	S8
G/TiO_2	3.0 / 0.15	0.51	—	2.0 C	630 (1000 cycles)	1.8-2.8		S9
		1.2		1.0 mA cm^{-2}	658 (250 cycles)		0.79	
TiO_2 NW/G	60 / —	3.2	62	0.2 C	1053 (200 cycles)	1.5-2.8	—	S10
TiO_2 NTs/GO	10 / —	0.6	70	0.1 C	850.7 (100 cycles)	1.5-3.0	—	S11
CBC/TiO_2	7.3 / —	1.5	—	2.0 C	475 (250 cycles)	1.8-2.8		S12
		4.0		3.35 mA cm^{-2}	453 (100 cycles)		1.81	
C@Ti_4O_7	148 / 2.8	1.5	63	2.0 C	562 (500 cycles)	1.7-3.0	—	S13
TiO–C65	7.5 / 0.7	2.0	—	2.0 C	533 (300 cycles)	1.8-2.8	—	S14
G-$Li_4Ti_5O_{12}$	35 / 0.346	1.0-1.2	60	1.0 C	697 (500 cycles)	1.7-2.8	—	S15
G/M@CNT	2.0 / 0.104	1.11-2.37	60-80	1.0 C	293 (2500 cycles)	1.8-2.6	—	S16
CNTs/V_2O_5RSL	15 / 0.4-0.6	2.0	50	1.0 C	939 (250 cycles)	1.7-2.8		S17
		6.0	70.4	2.0 mA cm^{-2}	~800 (100 cycles)		4.8	
HCNF and δ-MnO_2	2.0 / —	2.1	—	2.0 C	485 (400 cycles)	1.7-2.8		S18
		4.1	70	6.9 mA cm^{-2}	330 (100 cycles)		1.35	
MoO_3	— / 0.45	0.9-1.0	—	0.5 C	648.4 (200 cycles)	1.6-2.8		25
		2.2		3.7 mA cm^{-2}	700 (25 cycles)		1.54	
MoS_2/Celgard	0.35 / —	—	65	0.5 C	404 (600 cycles)	1.5-3.0	—	S19
$MgBO_2(OH)$/CNT	7.0 / —	1.1	70	0.5 C	785 (200 cycles)	1.8-2.8		S20
		4.1		1.4 mA cm^{-2}	710 (80 cycles)		2.91	
Co_9S_8	— / 0.16	2.0	70	1.0 C	530 (1000 cycles)	1.8-2.8		28
		5.6		—	830 (200 cycles)		4.6	
MoO_3@CNT	20 / 0.577	1.0	60	1.0 C	641 (400 cycles)	1.7-2.8	—	S21
CoP/KB	15.37 / 0.2	1.5	56	1.0 C	550 (500 cycles)	1.7-2.8		S22
		3.24		1.1 mA cm^{-2}	830 (100 cycles)		2.69	
MnO_2@PE	0.38 / 0.014	1.5	66	0.5 C	603 (500 cycles)	1.7-2.6		S23
		2.5		2.1 mA cm^{-2}	731.8 (100 cycles)		1.83	
UiO-66-NH_2@SiO_2	55 / —	0.5	—	0.1 C	600 (100 cycles)	1.6-3.0	—	S24
ZnO/GO	71.2 / 0.4	1.1-1.5	56	2.0 C	746.9 (300 cycles)	1.7-2.8		26
		3.5		1.2 mA cm^{-2}	838.8 (150 cycles)		2.94	

References

[S1] G. Liu, H. G. Yang, X. Wang, L. Cheng, J. Pan, G. Q. Lu, H.-M. Cheng, *J. Am. Chem. Soc.* **2009**, 131, 12868.

[S2] Kresse, G.; Furthmüller, *J. Phys. Rev. B* **1996**, 54, 11169.

[S3] Kresse, G.; Joubert, D. *Phys. Rev. B* **1999**, 59, 1758.

[S4] Perdew, J. P.; Burke, K.; Ernzerhof, M. *Phys. Rev. Lett.* **1996**, 77, 3865.

[S5] Grimme, S.; Antony, J.; Ehrlich, S.; Krieg, H. *J. Chem. Phys.* **2010**, 132, 154104.

[S6] Henkelman, G.; Uberuaga, B. P.; Jónsson, H. *J. Chem. Phys.* **2000**, 113, 9901.

[S7] H. B. Ding, Q. F. Zhang, Z. M. Liu, J. Wang, R. F. Ma, L. Fan, T. Wang, J. G. Zhao, J. M. Ge, X. L. Lu, X. Z. Yu, B. G. Lu, *Electrochimica Acta* **2018**, 284, 314.

[S8] H. Y. Shao, W. K. Wang, H. Zhang, A. B. Wang, X. N Chen, Y. Q. Huang, *J. Power Sources* **2018**, 378, 537.

[S9] Z. B. Xiao, Z. Yang, L. Wang, H. G. Nie, M. Zhong, Q. Q. Lai, X. J. Xu, L. J. Zhang and S. M. Huang, *Adv. Mater.* **2015**, 27, 2891.

[S10] G. M. Zhou, Y. B. Zhao, C. X. Zu, A. Manthiram, *Nano Energy* **2015**, 12, 240.

[S11] H. M. Song, C. Zuo, X. Q. Xu, Y. X. Wan, L. J. Wang, D. S. Zhou and Z. J. Chen, *RSC Adv.* **2018**, 8, 429.

[S12] F. Q. Lia, G. C. Wang, P. Wang, J. Yang, K. Zhang, Y. X. Liu, Y. Q. Lai, *J. Electroanalytical Chem.* **2017**, 788, 150.

[S13] H. Tang, S. S. Yao, S. K. Xue, M. Q. Liu, L. L. Chen, M. X. Jing, X. Q. Shen, T. B. Li, K. S. Xiao, S. B. Qin, *Electrochimica Acta* **201**8, 263, 158.

[S14] G. Y. Xu, Q.-B. Yan, S. T. Wang, A. Kushima, P. Bai, K. Liu, X. G. Zhang, Z. L. Tang and J. Li, *Chem. Sci.* **2017**, 8, 6619.

[S15] Y. Zhao, M. Liu, W. Lv, Y.-B. He, C. Wang, Q. B. Yun, B. H. Li, F. Y. Kang, Q.-H. Yang, *Nano Energy* **2016**, 30, 1.

[S16] W. B. Kong, L. J. Yan, Y. F. Luo, D. T. Wang, K. L. Jiang, Q. Q. Li, S. S. Fan and J. P. Wang, *Adv. Funct. Mater.* **2017**, 27, 1606663.

[S17] F. Liu, Q. F. Xiao, H. B. Wu, F. Sun, X. Y. Liu, F. Li, Z. Y. Le, L. Shen, G. Wang, M. Cai and Y. F. Lu, *ACS Nano* **2017**, 11, 2697.

[S18] Y. Q. Lai, P. Wang, F. R. Qin, M. Xu, J. Li, K. Zhang, Z. A. Zhang, *Energy Storage Mater.* **2017**, 9, 179.

[S19] Z. A. Ghazi, X. He, A. M. Khattak, N. A. Khan, B. Liang, A. Iqbal, J. X. Wang, H. Sin, L. S. Li and Z. Y. Tang, *Adv. Mater.* **2017**, 29, 1606817.

[S20] L. Kong, H.-J. Peng, J.-Q. Huang, W. C. Zhu, G. Zhang, Z.-W. Zhang, P.-Y. Zhai, P. P. Sun, J. Xie, Q. Zhang, *Energy Storage Mater.* **2017**, 8, 153.

[S21] L.Y. Luo, X. Y. Qin, J. X. Wu, G. M. Liang, Q. Li, M. Liu, F. Y. Kang, G. H. Chen and B. H. Li, *J. Mater. Chem. A* **2018**, 6, 8612.

[S22] X. X. Chen, X. Y. Ding, C. S. Wang, Z. Y. Feng, L. Q. Xu, X. Gao, Y. J. Zhai and D. B. Wang, *Nanoscale* **2018**, 10, 13694.

[S23] X. Song, G. P. Chen, S. Q. Wang, Y. P. Huang, Z. Y. Jiang, L.-X. Ding and H. H. Wang, *ACS Appl. Mater. Interfaces* **2018**, 10, 26274.

[S24] S. Suriyakumar, A. M. Stephan, N. Angulakshmi, M. H. Hassan and M. H. Alkordi, *J. Mater. Chem. A* **2018**, 6, 14623.